CrossMark

A Look at Outbursts of Comet C/2014 UN$_{271}$ (Bernardinelli–Bernstein) near 20 au

Michael S. P. Kelley[1], Rosita Kokotanekova[2,3], Carrie E. Holt[1], Silvia Protopapa[4], Dennis Bodewits[5],
Matthew M. Knight[6], Tim Lister[7], Helen Usher[8], Joseph Chatelain[7], Edward Gomez[9], Sarah Greenstreet[10],
Tony Angel[11], and Ben Wooding[12]

[1] Department of Astronomy, University of Maryland, College Park, MD 20742-0001, USA; msk@astro.umd.edu
[2] European Southern Observatory, Karl-Schwarzschild-Str 2, D-85748 Garching, Germany
[3] Institute of Astronomy and National Astronomical Observatory, Bulgarian Academy of Sciences, 72 Tsarigradsko shose Boulevard, 1784 Sofia, Bulgaria
[4] Southwest Research Institute, 1050 Walnut Street, Suite 300, Boulder, CO 80302, USA
[5] Physics Department, Leach Science Center, Auburn University, Auburn, AL 36849, USA
[6] Physics Department, United States Naval Academy, 572C Holloway Road, Annapolis, MD 21402, USA
[7] Las Cumbres Observatory, 6740 Cortona Drive, Suite 102, Goleta, CA 93117, USA
[8] The Open University, Walton Hall, Milton Keynes, MK7 6AA, UK
[9] Las Cumbres Observatory, School of Physics and Astronomy, Cardiff University, Queens Buildings, The Parade, Cardiff CF24 3AA, UK
[10] Department of Astronomy and the DIRAC Institute, University of Washington, 3910 15th Avenue NE, Seattle, WA 98195, USA
[11] Harlingten Observatory, Observatorio Sierra Contraviesa, Cortijo El Cerezo, Torvizcon 18430, Granada, Spain
[12] St Mary's Catholic Primary School, Llangewydd Road, Bridgend, Wales, CF31 4JW, UK

Abstract

Cometary activity may be driven by ices with very low sublimation temperatures, such as carbon monoxide ice, which can sublimate at distances well beyond 20 au. This point is emphasized by the discovery of the Oort cloud comet C/2014 UN$_{271}$ (Bernardinelli–Bernstein) and its observed activity out to ∼26 au. Through observations of this comet's optical brightness and behavior, we can potentially discern the drivers of activity in the outer solar system. We present a study of the activity of comet Bernardinelli–Bernstein with broad-band optical photometry taken at 19–20 au from the Sun (2021 June to 2022 February) as part of the LCO Outbursting Objects Key (LOOK) Project. Our analysis shows that the comet's optical brightness during this period was initially dominated by cometary outbursts, stochastic events that ejected ∼10^7 to ∼10^8 kg of material on short (<1 day) timescales. We present evidence for three such outbursts occurring in 2021 June and September. The nominal nuclear volumes excavated by these events are similar to the 10–100 m pit-shaped voids on the surfaces of short-period comet nuclei, as imaged by spacecraft. Two out of three Oort cloud comets observed at large pre-perihelion distances exhibit outburst behavior near 20 au, suggesting such events may be common in this population. In addition, quiescent CO-driven activity may account for the brightness of the comet in 2022 January to February, but that variations in the cometary active area (i.e., the amount of sublimating ice) with heliocentric distance are also possible.

Unified Astronomy Thesaurus concepts: Optical astronomy (1776); Broad band photometry (184); Long period comets (933); Coma dust (2159); Comet surfaces (2161)

Supporting material: machine-readable table

1. Introduction

Comet C/2014 UN$_{271}$ (Bernardinelli–Bernstein) was discovered in a search of the Dark Energy Survey data archive for new solar system objects (Bernardinelli et al. 2021). Originally designated as an asteroid, the object was found in data from 2014 to 2018, at heliocentric distances, r_h, of 29.0 to 23.7 au. Shortly after the discovery announcement in 2021 (Bernardinelli & Bernstein 2021), new observations at $r_h = 20$ au found the object to be extended and about –1.5 mag brighter than expected based on the 2014–2018 photometry, and the object was subsequently re-designated as a comet (Kokotanekova et al. 2021a; Buzzi et al. 2021). The object was serendipitously observed by the Transiting Exoplanet Survey Satellite (TESS) in 2018 and 2020, showing direct evidence for activity as far out as 23 au, and a lack of any periodic variability (Bernardinelli et al. 2021; Farnham et al. 2021; Ridden-Harper et al. 2021). A

reanalysis of the prediscovery data in the Dark Energy Survey and Panoramic Survey Telescope and Rapid Response System (PanSTARRS) archives confirmed activity out to ∼26 au (Bernardinelli et al. 2021). The comet is notable for being discovered at such a great distance (see Meech et al. 2017) and for its large size, estimated to be 69 ± 9 km in radius by Lellouch et al. (2022) and 60 ± 7 to 69 ± 8 km by Hui et al. (2022). It is the largest known Oort cloud comet nucleus, and second to 95P/Chiron (Ruprecht et al. 2015) for the largest cometary nucleus overall.

Little is known about cometary activity at ∼20 au. At such great distances, activity is likely driven by the sublimation of volatiles with low sublimation temperatures. The volatiles CO and CO_2, found in abundance in the cometary population (A'Hearn et al. 2012), have nominal sublimation temperatures of 25 and 80 K, respectively, although some level of sublimation can occur below these values (Meech & Svoreň 2004). The temperature of a blackbody sphere is $T \sim 60$ K at 20 au, which suggests CO sublimation can persist out to many tens of astronomical units, as long as ices are available near the nuclear surface. As an alternative to ice
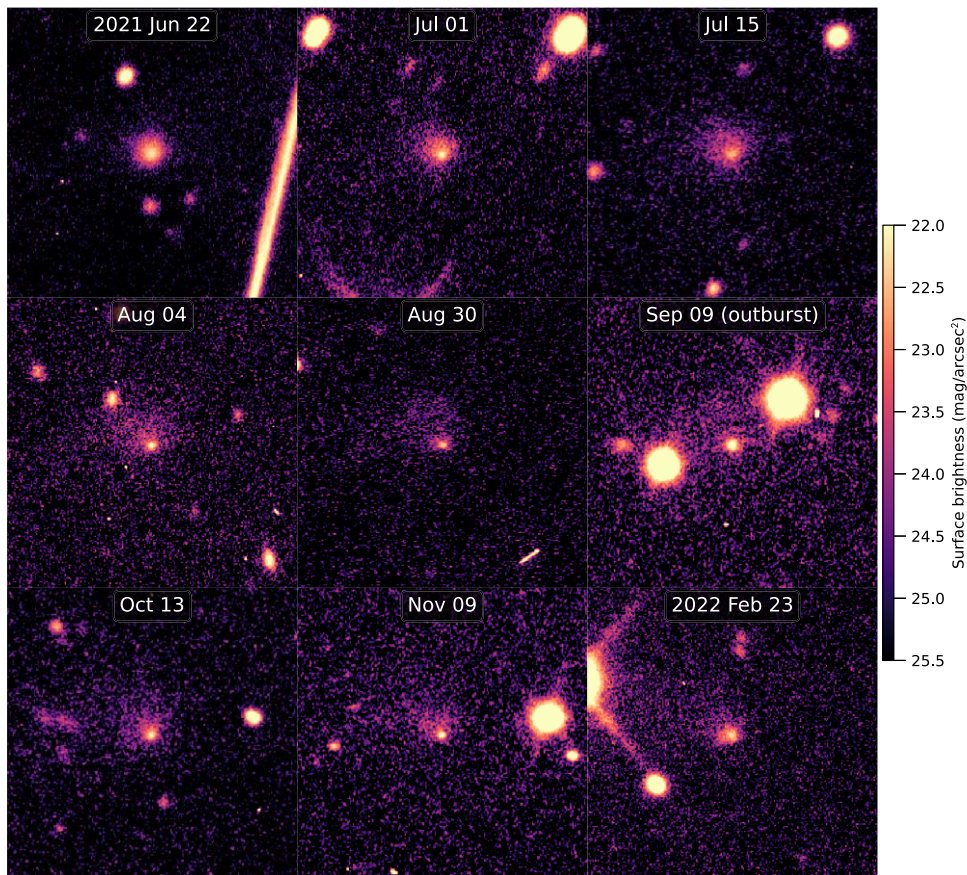
Figure 1. Select LCO images of comet C/2014 UN_{271} (Bernardinelli–Bernstein). Dates are as indicated, all images are through an r' filter, except on 2021 June 22, which is through w. All images are displayed with the same color scale and are 1,320,000 km × 1,320,000 km in size ($90''$ on 2021 June 22). Celestial north is up, east to the left. Over this time period, the heliocentric distance decreased from 21.78 to 19.28 au, the projected comet–Sun vector increased from position angle 46° to 292°, and the projected velocity vector increased from 144° to 153°.

sublimation, water-ice phase transitions may also drive cometary activity, but they are unlikely to be major contributors at such great distances (Jewitt et al. 2017). Aside from comet Bernardinelli–Bernstein, the three comets with the most distantly observed activities are C/1995 O1 (Hale-Bopp), active post-perihelion out to 27 au (Kramer et al. 2014); C/2010 U3 (Boattini), active pre-perihelion at 26 au (Hui et al. 2019); and C/2017 K2 (PanSTARRS), active pre-perihelion at 24 au (Hui et al. 2018).

We present images and photometry of comet Bernardinelli–Bernstein taken as part of the LCO Outbursting Objects Key Project (LOOK Project; Lister et al. 2022) using the Las Cumbres Observatory (LCO) global telescope network. We characterize the coma color, lightcurve, and morphology and show that the comet's activity near 20 au has varied substantially with time.

2. Observations and Reduction

Images of comet Bernardinelli–Bernstein were taken by our team and by schoolchildren in Wales as part of the Comet Chasers educational outreach program through the Faulkes Telescope Project. Observations were taken with LCO's 1 m robotic telescopes, specifically those located at Siding Spring Observatory, Australia; South African Astronomical Observatory, South Africa; and the Cerro Tololo Inter-American Observatory, Chile. Each telescope is equipped with identical Sinistro cameras, utilizing 4 k × 4 k CCDs with a nominal

pixel scale of $0''39$ and a suite of filters. For most observations, we used the SDSS g' and r' filters, although the w (effectively $g + r + i$), V, and R filters were used in a few circumstances. LOOK Project observing sequences were scheduled with the NEOExchange observation manager (Lister et al. 2021). The telescopes tracked the proper motion of the comet, and exposure times were typically 300 s with two exposures per filter.

Images were processed by LCO's BANZAI (Beautiful Algorithms to Normalize Zillions of Astronomical Images) pipeline (McCully et al. 2018), which includes bias, dark, and flat-field corrections, source extraction, and astrometric calibration. Individual frame exposure times were short enough that stars only trail by ~0.66–$0''71$ in 300 s exposures. We used the pipeline-produced source catalog to photometrically correct each image, calibrating them to the PanSTARRS 1 (PS1) photometric system (Tonry et al. 2012) using the ATLAS-RefCat2 photometric catalog (Tonry et al. 2018), and LOOK Project–derived color corrections. Details on the data reduction are presented by Lister et al. (2022). For this paper, we adopt the apparent magnitude and effective wavelengths for the solar spectrum from Willmer (2018): $g_{P1} = -26.54$ AB mag at 481.1 nm and $r_{P1} = -26.93$ AB mag at 615.6 nm (PS1 system photometry is hereafter denoted g and r). Sample images are presented in Figure 1.

Photometry of the comet was measured in coadded frames, grouped by telescope and time. We chose an aperture size of

Table 1
Observational Circumstances and Photometry

Date (UTC) (1)	Year (UTC) (2)	Filter (3)	Cal. (4)	r_h (au) (5)	Δ (au) (6)	θ (°) (7)	Airmass (8)	Seeing (″) (9)	N_{images} (10)	t_{exp} (s) (11)	m (mag) (12)	σ_m (mag) (13)	H_r (mag) (14)
2021-06-22 04:13	2021.472	w	r_{P1}	20.177	20.198	2.884	1.25	2.7	3	900	18.275	0.068	5.098
2021-09-08 02:33	2021.685	r'	r_{P1}	19.892	19.448	2.636	1.09	1.6	1	300	19.239	0.102	6.185
2021-09-09 22:04	2021.690	g'	g_{P1}	19.886	19.438	2.631	1.45	1.9	2	600	19.090	0.072	5.564
2021-09-18 02:09	2021.713	r'	r_{P1}	19.856	19.401	2.617	1.10	2.2	2	600	18.786	0.075	5.742
2021-09-23 05:03	2021.727	r'	r_{P1}	19.837	19.382	2.615	1.21	1.8	2	600	18.645	0.070	5.606
2021-10-07 21:40	2021.767	r'	r_{P1}	19.783	19.349	2.637	1.21	1.7	2	600	18.883	0.065	5.852
2021-11-05 19:45	2021.846	r'	r_{P1}	19.678	19.367	2.764	1.21	2.0	1	300	19.086	0.096	6.059
2021-12-10 19:21	2021.942	r'	r_{P1}	19.550	19.491	2.886	1.10	2.1	2	600	19.135	0.073	6.103
2022-01-11 12:57	2022.029	r'	r_{P1}	19.434	19.624	2.832	1.52	3.0	2	600	19.184	0.080	6.153
2022-02-14 01:28	2022.121	r'	r_{P1}	19.312	19.700	2.667	1.55	2.6	2	600	18.948	0.082	5.929

Note. Column descriptions: (1) midtime of the observation; (2) midtime as fractional year; (3) filter used in the observation; (4) PS1 filter to which the photometry is calibrated; (5) heliocentric distance; (6) observer–target distance; (7) Sun–target–observer (phase) angle; (8) calculated airmass of the observation; (9) FWHM of point sources; (10) number of images; (11) total exposure time; (12) apparent magnitude; (13) uncertainty on the apparent magnitude; (14) absolute magnitude in the r band (g-band photometry has been scaled by the average color).

(This table is available in its entirety in machine-readable form.)

$6.''0$ (86,000 to 88,000 km at the comet; background annulus 20–40″) and limited our analysis to images with point-source FWHMs $<3''$ and final photometric uncertainties of <0.15 mag. We have 179 photometric measurements in 96 distinct observational epochs. Our first observation was on 2021 June 22 with the comet at a heliocentric distance $r_h = 20.18$ au, a geocentric distance $\Delta = 20.20$ au, and a Sun–target–observer (phase) angle $\theta = 2.°9$. Our last observation presented in this paper was on 2022 February 23 at $r_h = 19.28$ au, $\Delta = 19.70$ au, and $\theta = 2.°6$. The observational circumstances and photometry are presented in Table 1.

3. Results and Analysis

3.1. Color

Based on 70 photometry sets with contemporaneously obtained g- and r-band photometry, we find a weighted-mean coma color of $g - r = 0.47 \pm 0.01$ mag. All color sets are consistent with the mean at the 1.7σ level. There is no evidence for a trend with time or brightness (Pearson and Spearman correlation test p-values $\gg 0.05$). The color of the coma corresponds to a spectral gradient (A'Hearn et al. 1984) of $S_{g,r} = 5.48 \pm 0.05\%$ per 100 nm, where subscripts denote the PS1 bandpasses upon which the calculation is based.

The comparison between the coma color of comet Bernardinelli–Bernstein and those of other active long-period comets (LPCs; Solontoi et al. 2012; Jewitt 2015) is shown in Figure 2. The comparison is made in terms of the $V - R$ color for convenience only. Using the relations reported by Tonry et al. (2012), the $g - r$ color of comet Bernardinelli–Bernstein corresponds to $V - R = 0.43 \pm 0.02$ mag, which agrees within 2σ of the mean color of active LPCs: $V - R = 0.47 \pm 0.01$ mag (derived from data by Solontoi et al. 2012 and Jewitt 2015, and filter transformations by Ivezić et al. 2007). Therefore, comet Bernardinelli–Bernstein is a nominal LPC in terms of coma color. For comparison, the nucleus color of the comet measured by Bernardinelli et al. (2021) is $V - R = 0.40 \pm 0.02$ mag (also shown in Figure 2; color transformed following Abbott et al. 2021). The nucleus and coma colors are consistent at the 2σ level, with the nucleus being potentially bluer than the coma. This relationship between the colors of the coma and nucleus

environments is in agreement with the average colors reported by Jewitt (2015) for active and inactive LPCs.

3.2. Brightness and Lightcurve

In our first image of the comet, the spatial distribution is relatively compact, and a total brightness may be estimated. Within an $8.''9$ radius aperture (130,000 km), offset from the nucleus to make a tight fit around the visible dust, we measure $r = 18.14 \pm 0.07$ mag. Converting this brightness to an r-band absolute magnitude is done by scaling it to $r_h = 1$ au, $\Delta = 1$ au, and to a phase angle of $0°$ using the Schleicher–Marcus phase function for cometary dust (Schleicher & Bair 2011), yielding $H_r (1, 1, 0) = 4.96$ mag.

In Figure 3, we present the lightcurve of the comet as absolute magnitude versus time based on our full photometric data set. Initially, the comet's intrinsic brightness decreased with time, with the absolute magnitude in our photometric aperture increasing from 5.10 ± 0.07 mag (2021 June 22) to 6.11 ± 0.04 mag (2021 September 3–8). This fading period was followed by two brightening events. The brightening events are likely outbursts, the first occurring between 2021 September 8 02:33 and September 9 22:04 UTC (Kelley et al. 2021) and the second between September 18 02:09 and September 23 04:58 UTC.

With a functional form of the lightcurve, we can characterize the coma fading and the September outburst strengths. The absolute magnitude within the $6''$ radius aperture faded at a rate of 13.8 ± 0.4 mmag day^{-1} ($\chi_\nu^2 = 0.6$, rms $= 64$ mmag) from 2021 June 22 to September 8. The September 9 outburst's relative strength is -0.65 ± 0.07 mag and the absolute magnitude of the new material is $H_r = 6.32$ mag. The September 23 outburst strength is derived by comparing pre- and post-outburst r-band data, accounting for the linear decline in brightness: $\Delta m = -0.22 \pm 0.07$ mag, $H_r = 7.23$ mag. Differencing pre- and post-outburst images indicates that the photometric apertures at the time of the outburst discoveries include all of the new ejecta. We find no evidence for any other outbursts during this initial fading period. Each outburst is followed by a decline in coma brightness, likely due to the
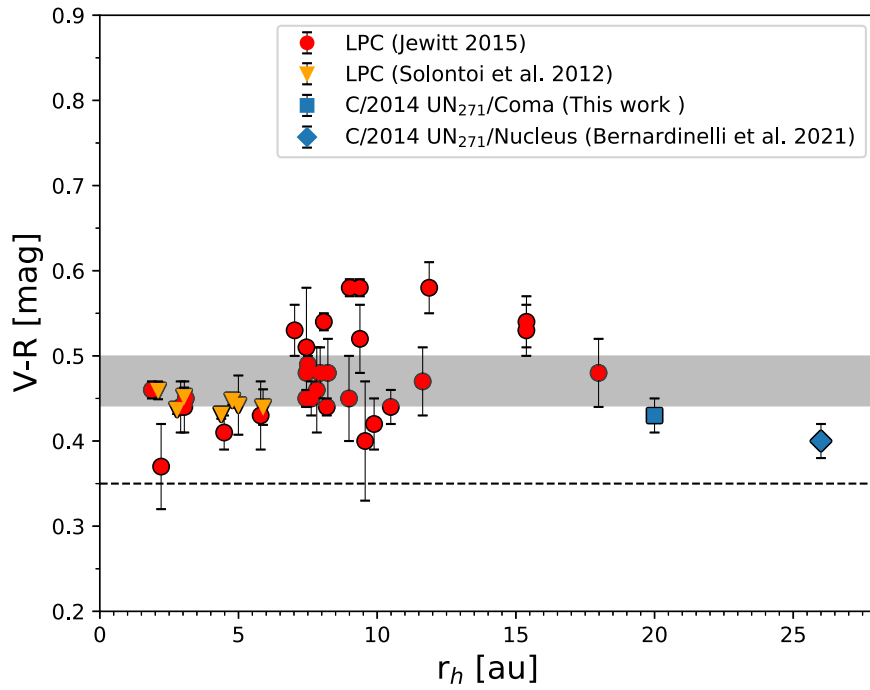
Figure 2. $V - R$ color as a function of heliocentric distance, r_h, comparing the color of the coma of comet C/2014 UN$_{271}$ (Bernardinelli–Bernstein) as measured in this work (square symbol) and that of other active LPCs from Jewitt (2015) and Solontoi et al. (2012). The gray rectangle defines the 3σ limits around the average $V - R$ color of active LPCs (0.47 ± 0.01 mag), and the horizontal dashed line is the color of the Sun. Color-wise, comet Bernardinelli–Bernstein is a typical active LPC. The color of the nucleus (Bernardinelli et al. 2021) is also shown for comparison (diamond).

Figure 3. Absolute magnitude, H_r (1, 1, 0), of comet C/2014 UN$_{271}$ (Bernardinelli–Bernstein) measured within $6''$ radius apertures from LOOK Project photometry (g band as circles, r band as squares) versus time. Data calibrated to the g-band have been scaled with the measured coma colors to make an effective r-band data set. The brightness of the coma from PanSTARRS 1 (PS1) data measured on 2019.66 UTC, using the same aperture size, is marked with a dotted line, and the absolute magnitude of the nucleus is given as a dashed line (Bernardinelli et al. 2021).

expansion of the ejecta and any prior released material beyond the photometric aperture.

Following the outbursts was a period of low-amplitude variability that started in October, with a mean $H_r = 5.98 \pm 0.01$ mag but an rms of 0.12 mag (19 r-band photometric data points between 2021 October 7 and 2022 February 23). The variability appears to be smooth with time,

but gaps in the data could hide small, ∼–0.1 mag outbursts. Monthly averaged absolute magnitudes are $H_r = 5.87 \pm 0.02$, 6.06 ± 0.03, 6.19 ± 0.05, 6.06 ± 0.04, and 5.94 ± 0.05 mag for 2021 October, November, and December; and 2022 January and February, respectively. Some of the fading from October to November may still be due to residual ejecta from the September outbursts but without a dynamical model or
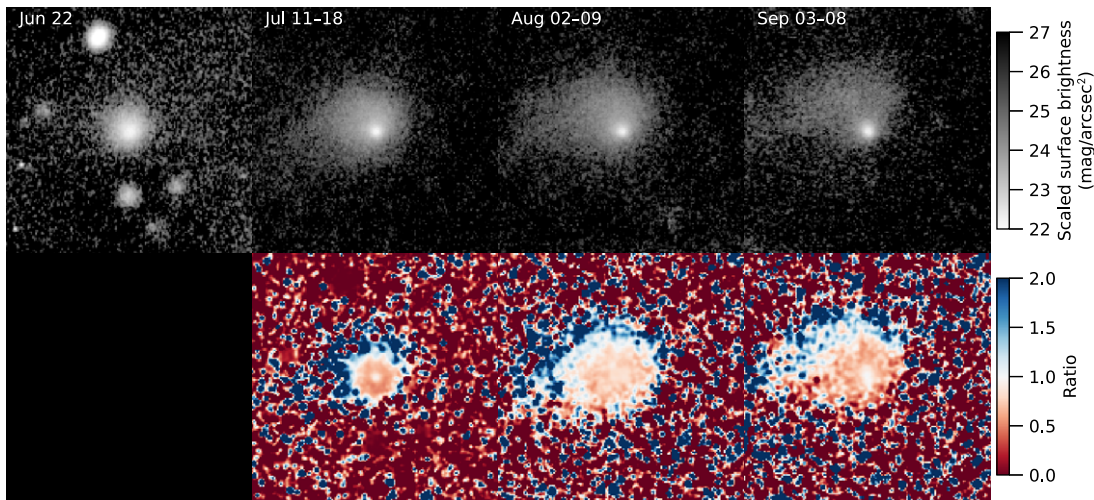
Figure 4. Top: LCO images of comet C/2014 UN$_{271}$ (Bernardinelli–Bernstein). Dates (2021) are as indicated. Except for the image on June 22, which is a single night w-band average, images are median-combined g' and r' data taken over a range of dates: 2021 July 11–18, August 2–9, and September 3–8. All images are displayed with the same photometric color scale and show an area of 880,000 km × 880,000 km (60″ on 2021 June 22). Bottom: The same images, but normalized by the previous image in the sequence and smoothed with a $\sigma = 1$ pixel Gaussian filter. The expanding morphology of the comet is apparent throughout this period.

higher-spatial-resolution data, or some assessment of possible quiescent activity, this interpretation is speculation. We will return to this point in Section 4.2.

3.3. Dust Cross-sectional Area and Mass

With assumptions on the dust and/or ice-grain properties, absolute magnitudes may be converted into total cross-sectional area and mass. We initially assume all grains have the same properties: effective radius $a_{\rm eff} = 10\,\mu$m, grain mass density of $\rho_g = 1.0\,\mathrm{kg\,m^{-3}}$, and r-band albedo $A_r = 4\%$. The albedo is a nominal value that is similar to the nucleus surface (Hui et al. 2022), and the grain mass density allows for porous dust grains and/or the presence of water ice. Thus, the absolute magnitudes of the total coma in June 2021 and the ejecta of the two outbursts in September 2021 ($H_r = 4.96 \pm 0.07$, 6.32 ± 0.07, and 7.23 ± 0.07 mag) correspond to cross-sectional areas $G = 3.1 \times 10^5$, 0.88×10^5, and 0.38×10^5 km^2, and masses $M = 4.1 \times 10^8$, 1.2×10^8, and 0.51×10^8 kg, respectively (6% formal uncertainties on all values). There is considerable uncertainty in the adopted grain parameters, which greatly affects the mass estimates. The mass scales with the quantity $a_{\rm eff}\,\rho_g/A_p$. Effective grain radius has the largest effect, as sizes of 1 or 100 μm, or even a size distribution, could have been chosen. We take $a_{\rm eff} = 10\,\mu$m as our nominal case (equivalent to a differential size distribution $\propto a^{-3.5}$ for a between 1 and 100 μm; see, e.g., Ishiguro et al. 2016) and assume a factor of 10 in the mass uncertainty (see Tubiana et al. 2015).

3.4. Morphological Evolution

The comet's morphology changed during the initial fading period (2021 June 22–September 8). To quantitatively evaluate these changes, we median-combined g' and r' images taken over the time periods July 11–18, August 3–8, and September 3–8. Figure 4 presents the results. The time sequence suggests an expanding morphology. To emphasize the variation, we divided each image by the previous image in the sequence and show the results in Figure 4. The ratio confirms the expansion.

A projected dust expansion speed can be estimated using the coadded images in Figure 4. We generated a detection mask on each image, identifying the coma using a 3×3 pixel moving box where at least 1 pixel is more than 2σ from the background. Assuming radial motion, the coma edge expands at a rate of 48 to 84 m s^{-1} (approximately monotonically increasing from $-50°$ to $+100°$ east of north) for the time period 2021 June 22 to July 14. The expansion rate is nonlinear with time in our data, falling to near 0 or even negative values thereafter, at least for this edge-detection method. However, this approach does not track any one single feature, but instead the edge of the detected coma, which depends on the image signal-to-noise ratio and the actual surface brightness distribution of the coma. Furthermore, the expansion may not be radial, and solar radiation pressure or Lorentz forces may be accelerating the dust (e.g., Hui et al. 2019). At best we have estimated the order of magnitude of the initial mean expansion speed, at worst we have measured a lower limit to the fastest moving material. In addition, an estimate of the slowest material may be made using the lightcurve. The slowest ejecta takes at least 78 days to move 6″, thereby moving $\leqslant 13$ m s^{-1} in projection on the sky.

Mean surface brightness (S_ν) profiles as a function of distance to the nucleus (ρ) show a morphological evolution of the initial coma (Figure 5). The mean profile of the comet flattens with time. Assuming a functional form of $S_\nu \propto \rho^k$, the best-fit slopes between 3″ to 10″ are $k = -2.63 \pm 0.06$, -1.22 ± 0.02, -0.99 ± 0.02, and -0.90 ± 0.03 for the time periods 2021 June 22, July 11–18, August 02–09, and September 3–8, respectively.

Also included in Figure 5 are mean radial profiles for images generated by combining data month by month from 2021 October to 2022 February. At 3″ to 10″, the best-fit radial profile slopes are all steeper than -1: -1.39 ± 0.04, -1.26 ± 0.06, -1.27 ± 0.08, -1.71 ± 0.06, and -1.76 ± 0.06, for 2021 October, November, and December; and 2022 January and February, respectively. Despite the 50–120 day time period since the last outburst, the coma does not appear to be in a steady state, and even steepened as the comet brightened in 2022.

4. Discussion

We have characterized the lightcurve and morphology of comet C/2014 UN$_{271}$ (Bernardinelli–Bernstein) from 2021
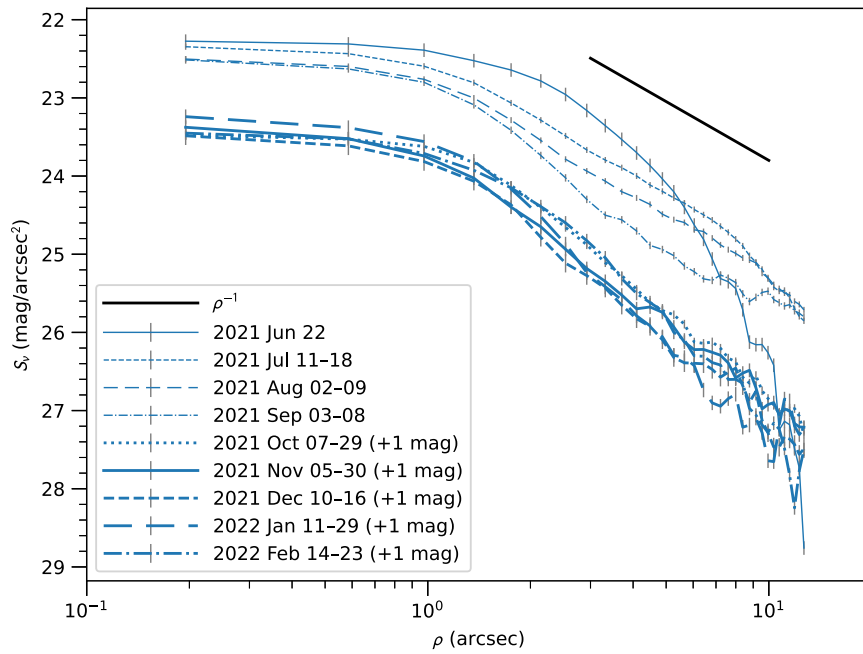
5

Figure 5. Surface brightness (S_ν) profiles as a function of distance to the nucleus (ρ) for the images presented in Figure 4. The profile of the comet is initially steep but flattens with time. A nominal coma profile, ρ^{-1}, is shown for reference. The mean seeing of these images is $1''\!.8$. Also shown are the monthly mean profiles from 2021 October to 2022 February, offset by $+1$ mag for clarity (mean seeing $2''\!.3$).

June 22 to 2022 February 23, in an effort to help increase our knowledge of the activity of comets near 20 au. We now synthesize the results to better understand the state of activity of this particular comet and compare them to previous work regarding its activity.

4.1. Outbursts near 20 au

Following our first detection of the comet on 2021 June 22, the intrinsic brightness faded, the morphology expanded, and the mean radial profile flattened with time. Together, these are the signatures of material ejected by a cometary outburst leaving the vicinity of the nucleus. In contrast, a steady-state coma would have a surface brightness profile proportional to ρ^{-1}. A steep initial slope, $k < -1$, indicates a rapid ejection of new material into the unresolved source. The fading with time shows that the driver of this new material had ceased, or at least rapidly decreased compared to the timescale of dust expansion. That the radial profile flattened as the brightness decreased in our photometric aperture is due to the expansion of the material on the sky. The slope just before the first September outburst, $k = -0.9$, suggests the coma might have been near a steady state at that time, but due to the September outbursts, we could not study the evolution any further to confirm this point (e.g., the profile may have continued to flatten with the expansion of the material). Therefore, we conclude that the appearance of the comet from 2021 June 22 to September 8 is dominated by an outburst occurring before our first observation.

If these data were instead observations of a previously steady-state coma that had suddenly ceased activity on or about 2021 June 22, then the radial profile would have initially been near -1, rather than <-2, as observed. Alternatively, if the comet activity had rapidly increased to establish a new quiescent level by 2021 September, then an initially steep radial profile could have been observed, trending toward -1 with time. However, in this case, the comet would have brightened, not faded with time.

Bernardinelli et al. (2021) measured the integrated brightness of the comet in PanSTARRS 1 images taken on 2019 August 29 UTC at 22.6 au, 663 days before our first image at 20.2 au. Their value, $H_r = 6.5$ mag in a $6''$ radius aperture, compares favorably with our minimum brightness in 2021 September, $H_r = 6.1$ mag. Thus, our suggestion that the radial profile at $3''$–$10''$ in 2021 September was trending toward a steady-state coma is possible. However, in 2021 November–2022 February, when the comet was at a similar brightness ($H_r = 6.2$ to 5.9 mag), the radial profile slope was -1.3 to -1.8, significantly steeper than -1. We suggest residual ejecta from the September outbursts affect the spatial profile in November–December. Additional small (~ -0.1 mag) outbursts may have caused the ~ -0.25 mag brightening between 2021 December 16 and 2022 February 23. Validation of this hypothesis would benefit from additional data that could establish the quiescent behavior of the comet.

A comparison of the PS1 photometry from 2019 August to the total coma brightness measured in our first image ($H_r = 4.96$ mag) indicates that the outburst preceding our initial observations of this comet was likely no stronger than $\Delta m = -1.5$ mag ($6''$ radius aperture). Based on the rapid evolution of the ejecta from 2021 June 22 to July 11–18 (~ 50 m s^{-1} expansion speed), the outburst likely occurred in the month before our first observation. In Section 3.3, we estimated the total mass of the observed dust on 2021 June 22 to be 4×10^8 kg, with uncertainties of a factor of 10 due to unknown grain properties. Removing the PS1 measurement as a possible ambient coma reduces the nominal mass to 3×10^8 kg, which does not affect the order of magnitude estimate. In a summary of 17 outbursts over an ~ 8 yr period, Ishiguro et al. (2016) found three events (18%) with cross-sectional areas similar to or larger than our nominal estimate, indicating that this very large cometary nucleus at 20 au has outbursts as large as any typical comet near 1 au. Outbursts of this scale correspond to equivalent nuclear volumes of cylindrical pits

with diameter $D = 80(m/10^8 \, \text{kg})^{1/3}$ m (assuming a bulk nucleus density of $500 \, \text{kg} \, \text{m}^{-3}$ and a depth-to-diameter ratio of 0.5). The size of the excavated region is only weakly affected by our large mass uncertainties; a factor of 10 uncertainty in mass corresponds to a factor of 2 uncertainty in diameter. Therefore, such surface features would be comparable to the pits observed on the surfaces of comets 9P/Tempel 1, 67P/Churyumov-Gerasimenko, and 81P/Wild 2 (Brownlee et al. 2004; Veverka et al. 2013; Vincent et al. 2015).

Without a direct spectroscopic detection of a gas, we cannot determine with certainty what drove the outbursts, or if they were mechanical or thermophysical in nature (i.e., due to thermal cracking, or landslides). We can likely rule out amorphous to crystalline transitions of water ice as Jewitt et al. (2017) estimated that they most likely occur within 12.5 au from the Sun for comets (outside of this distance crystallization timescales are too long). Carbon monoxide ice is the most likely driver of activity and outbursts at 20 au, being that it is both abundant in the cometary population (Cochran et al. 2015) and volatile at this distance (Meech & Svoreň 2004). While CO has been observed in distant comets (Wierzchos et al. 2017; Womack et al. 2017; Yang et al. 2021), the relationship between CO and outbursts is not clear, even in the best-observed outbursting comet 29P/Schwassmann-Wachmann 1. Wierzchos & Womack (2020) could not identify a strong correlation between their CO and optical lightcurves of comet 29P and concluded that increases in CO-outgassing are not always involved with the optically identified outbursts.

4.2. Quiescent Activity and Drivers

Comet Bernardinelli–Bernstein was clearly active beyond $r_h = 20$ au (Section 1). Persistent, distant activity of comets is typically attributed to the sublimation of species more volatile than H_2O, whose sublimation rates drop off significantly for $r_h > 2.5$ au. Bernardinelli et al. (2021) estimated the ice responsible for cometary activity, based on photometry of the coma from $r_h = 29$ to 20 au and thermal models of the nuclear surface. They concluded that the increase of brightness grew rapidly with heliocentric distance and was consistent with the sublimation of CO_2 ice. However, their data set included photometry from 2021 June, which we have shown is substantially affected by an outburst that ejected $10^7 - 10^9$ kg of material. This outburst brightened the coma within $6''$ by a factor of 3 to 4, as observed on June 22. This calls into question the conclusion that CO_2 is the responsible volatile or at least requires a reanalysis of the activity without using the 2021 data.

The analysis of Hubble Space Telescope data taken 2022 January 8 by Hui et al. (2022) shows that the inner coma ($\rho < 1''$) has logarithmic radial slopes ranging from -1.7 to ~ -1.0 and is steepest in the direction of the Sun. Remarking that a slope of -1.5 is expected in the sunward direction due to radiation pressure, they conclude the observations are consistent with a steady-state coma. In our observations, the absolute magnitude of the comet on 2022 January 11 is consistent with the 2022 December average ($H_r = 6.15 \pm 0.08$ mag and 6.19 ± 0.05 mag, respectively). Therefore, the brightening seen in 2022 likely occurs after this date and the conclusions of Hui et al. (2022) are not inconsistent with our own. In fact, it may indicate that our 2021 December photometry is dominated by a quiescent activity state.

To assess the contribution of quiescent activity to our data, we have developed an ad hoc model with illustrative functional forms for each contribution: three outbursts and a quiescent coma. All three outbursts are considered to be step functions with an exponential falloff in dust cross section (i.e., magnitude increases linearly with time). For simplicity, the decay timescales are identical for each event. For the quiescent activity, we take a standard approach in cometary astronomy by assuming the activity scales as a power-law function of heliocentric distance: r_h^k. We derived the power-law exponent from CO-ice sublimation rates calculated with the Cowan & A'Hearn (1979) ice sublimation model. Fits to the model CO sublimation rates between 18 and 26 au yield slopes ranging from -2.2 for a slowly rotating nucleus to -2.4 for a rapidly rotating nucleus (we assumed a constant active area and a 5% albedo over all wavelengths; best-fit residuals were $<1\%$). The dust production rate is assumed to be directly proportional to the CO sublimation rate and scaled to the PS1 photometry from 2019 August 28. The outburst strengths and decay timescales are manually adjusted, and the result is shown in Figure 6.

The model lightcurve has poor agreement with the first outburst, either due to our chosen outburst functional form (linear in magnitude space) or to the amount of quiescent activity ($H = 6.2$ mag on 2021 September 8). Here, an outburst decay timescale of $\tau = 24$ days is shown. Longer timescales would better fit the July–August photometry but require a shallower heliocentric distance slope for the quiescent activity in order to fit the early September data points. However, the quiescent activity is already well below the 2022 January–February photometry ($\Delta H > 0.1$ mag), and a shallower slope would cause greater disagreement. In addition, the assumption that the activity has been growing following the PS1 measurement in 2019 could be incorrect, or that some other effect is needed to match the 2022 data, such as the small outbursts suggested in Section 4.1. Furthermore, large aperture photometry from TESS by Bernardinelli et al. (2021) indicate 1.5 ± 0.2 mag of brightening from $r_h = 23.8$ to 21.2 au (2018 October to 2020 September), more consistent with activity proportional to r_h^{-12} than $r_h^{-2.2}$, or with additional prediscovery outbursts, which calls into question whether or not the PS1 data at 22.6 au are appropriate for establishing a quiescent activity level. Altogether, the model suggests that CO-ice-driven sublimation is possible but some other model assumption must be challenged to confirm this conclusion.

As an alternative to slowly increasing sublimation driven mass loss from CO, we present a second model for the quiescent activity in Figure 6. Here, we leave the activity as constant since the PS1 measurement, then add a linearly increasing enhancement starting in early October. This model has a much better agreement with the data. The outburst decay timescale, $\tau = 40$ days, is long enough for the lightcurve to be nearly linear in July–August, consistent with the data. Moreover, the local minimum in brightness in 2021 December is reproduced, along with the brightening trend in 2022. We have no particular physical motivation for this model, other than the possibility that the outbursts signaled the onset of a new active area, perhaps due to the propagation of heat into the subsurface as the comet approaches the Sun.

Taken together, our illustrative models in Figure 6 indicate that the lightcurve is outburst dominated from 2021 June through September and likely quiescent activity dominated by 2021 December. Observations with the Hubble Space Telescope in 2022 January support this conclusion, and the early assessment that the comet's activity was driven by CO_2
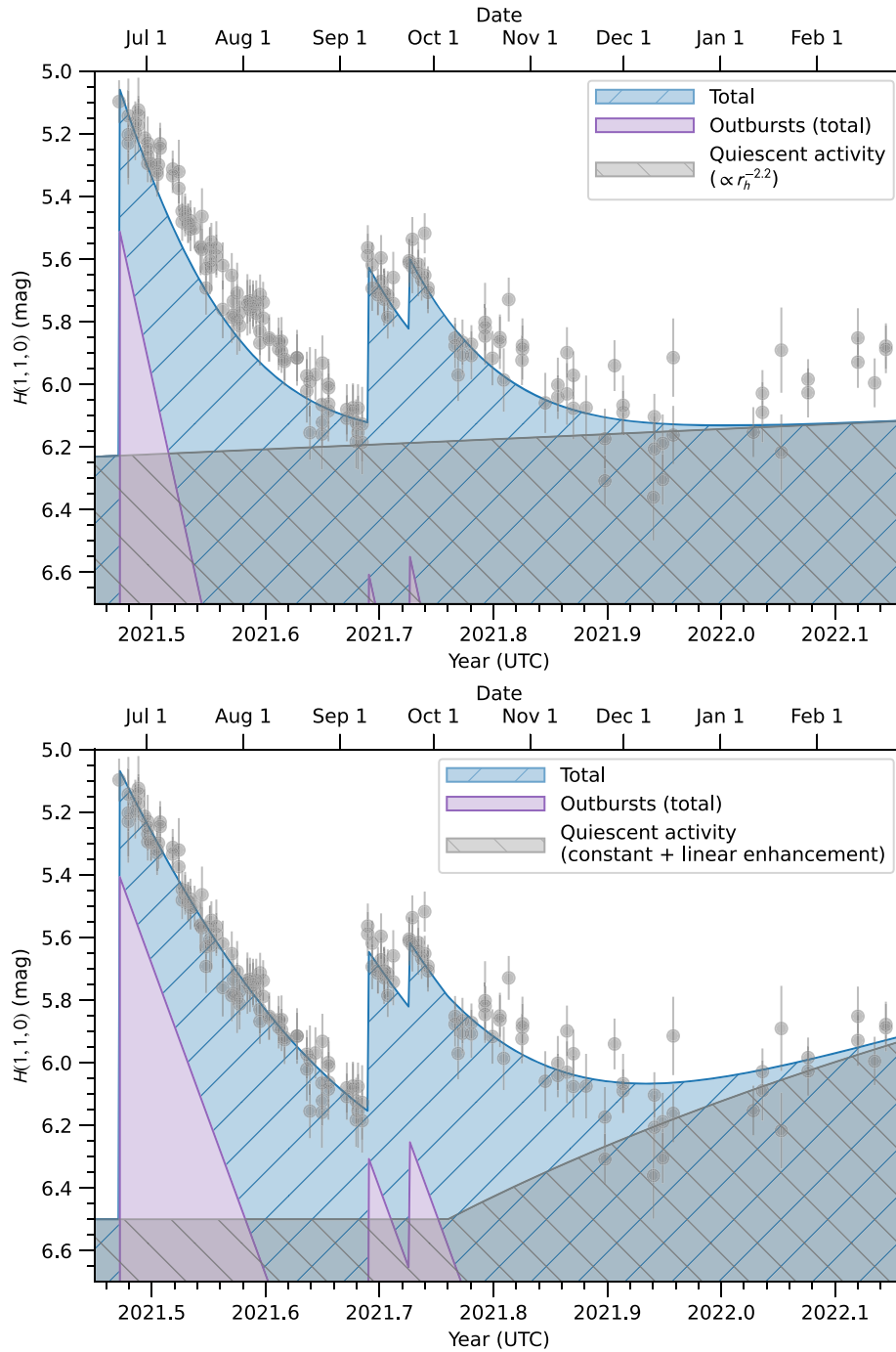
Figure 6. Ad hoc model lightcurves (absolute magnitude, $H(1, 1, 0)$ versus time) based on illustrative functional forms for the outbursts and quiescent activity of comet C/2014 UN$_{271}$ (Bernardinelli–Bernstein). LOOK Project photometry of the comet is shown as gray circles (g has been scaled to r as in Figure 4). Outbursts follow an exponential decay in dust cross section, with the same decay timescale, τ, for all events within a panel. Quiescent activity models are scaled to match the PS1 photometry from 2019 August 28. Top: quiescent activity model based on model CO-ice sublimation rates, Z, parameterized as $Z \propto r_h^{-2.2}$. Bottom: quiescent activity model based on constant activity since 2019 and a linearly increasing enhancement starting at 2021.76 (2021 October 5). Together, the models indicate that the lightcurve is outburst dominated but transitions to quiescent activity dominated by 2021 December.

sublimation, which partially relied on outburst-dominated photometry from 2021 June, is unlikely and needs revision.

5. Conclusions

We examined the intrinsic brightness of comet C/2014 UN$_{271}$ (Bernardinelli–Bernstein) as part of a study of this comet's distant activity. Our data set was comprised of g'- and r'-band images from the LOOK Project, including data from the Comet Chasers outreach program, over the time period from the discovery of activity on 2021 June 22 to 2022 February 23. Within $6''$ radius apertures, the comet had brightened by $\Delta m = -1.5$ mag between the last small-aperture photometric measurements in 2019 August from the PanSTARRS 1 survey (Bernardinelli et al. 2021) and the first LOOK Project photometric data on 2021 June 22. The absolute magnitude faded with time at a rate of 13.8 ± 0.4 mmag day^{-1},

up until two small outbursts on our about 2021 September 9 and 18 ($\Delta m = -0.65$ and -0.22 mag). The two smaller outbursts occurred while material from the June outburst was still expanding and leaving the aperture, i.e., the September outbursts happened before the quiescent coma state was reached. These events were immediately followed by a slight fading in intrinsic brightness ($+0.26$ mag), then a period of low-amplitude variability ($H_r = 5.9$ to 6.2 mag), up to the end of our data set. Radial profiles of the coma suggest the variability may be caused by small, ~ -0.1 mag outbursts, although no direct photometric evidence (e.g., a short-scale discontinuity in the lightcurve) is seen. A comparison of our data to the Hubble Space Telescope observations on 2022 January 08 (Hui et al. 2022) suggests our photometry in 2021 December was dominated by the quiescent coma, and an ad hoc analysis of our lightcurve confirms this point. Ejecta from the first (prior to 2021 June 22) outburst expanded with speeds of at least $50\,\mathrm{m\,s^{-1}}$ in the plane of the sky, and the slowest-moving ejecta no faster than $13\,\mathrm{m\,s^{-1}}$. Throughout the observed period, the color of the comet was constant (mean $g - r = 0.47 \pm 0.01$ mag) and consistent with the LPC population.

A pre-perihelion outburst ($\Delta m \sim -0.5$ mag) near $r_h \sim 20$ au was also observed at comet C/2010 U3 (Boattini) by Hui et al. (2019). It may be that pre-perihelion outbursts are common for Oort cloud comets in the outer solar system, although none have been reported for the third comet observed at these distances: comet C/2017 K2 (Jewitt et al. 2017; Meech et al. 2017; Hui et al. 2018). The nuclei of comets Bernardinelli–Bernstein and Boattini are likely complex geological worlds, and the cause(s) of these events may be difficult to discern at the present time. However, further study of cometary activity and outbursts at large heliocentric distances will be beneficial to understanding the long-term surface evolution (e.g., pit formation) of these comets and how it relates to the paucity of Oort cloud comet discoveries (i.e., the long-period comet fading phenomenon; Vokrouhlický et al. 2019; Kaib 2022). Furthermore, combining future observations with the pre-2021 data or observations with higher signal-to-noise ratios and finer spatial resolving powers may reveal more about the quiescent activity in this particular comet (e.g., Kokotanekova et al. 2021b; Hui et al. 2022).

Facilities: LCOGT.

Software: astropy (Astropy Collaboration et al. 2018), sbpy (Mommert et al. 2019), astroquery (Ginsburg et al. 2019), JPL Horizons (Giorgini et al. 1996), SEP (Barbary 2016), DS9 (Joye & Mandel 2003), reproject (Robitaille et al. 2020), photutils (Bradley et al. 2021), calviacat (Kelley & Lister 2019), ccdproc (Craig et al. 2021), BANZAI (McCully et al. 2018), fastrot (Van Selous & Kelley 2021).

ORCID iDs

Michael S. P. Kelley https://orcid.org/0000-0002-6702-7676
Rosita Kokotanekova https://orcid.org/0000-0003-4617-8878
Carrie E. Holt https://orcid.org/0000-0002-4043-6445
Silvia Protopapa https://orcid.org/0000-0001-8541-8550
Dennis Bodewits https://orcid.org/0000-0002-2668-7248
Matthew M. Knight https://orcid.org/0000-0003-2781-6897
Tim Lister https://orcid.org/0000-0002-3818-7769
Helen Usher https://orcid.org/0000-0002-8658-5534
Joseph Chatelain https://orcid.org/0000-0002-1278-5998
Edward Gomez https://orcid.org/0000-0001-5749-1507
Sarah Greenstreet https://orcid.org/0000-0002-4439-1539
Tony Angel https://orcid.org/0000-0003-4881-6255
Ben Wooding https://orcid.org/0000-0003-4227-0415

References

Abbott, T. M. C., Adamów, M., Aguena, M., et al. 2021, ApJS, 255, 20
A'Hearn, M. F., Feaga, L. M., Keller, H. U., et al. 2012, ApJ, 758, 29
A'Hearn, M. F., Schleicher, D. G., Millis, R. L., Feldman, P. D., & Thompson, D. T. 1984, AJ, 89, 579
Astropy Collaboration, Price-Whelan, A. M., & Sipőcz, B. M. 2018, AJ, 156, 123
Barbary, K. 2016, JOSS, 1, 58
Bernardinelli, P., & Bernstein, C. 2021, MPEC, 2021–M53
Bernardinelli, P. H., Bernstein, G. M., Montet, B. T., et al. 2021, ApJL, 921, L37
Bradley, L., Sipocz, B., Robitaille, T., et al. 2021, astropy/photutils: 1.1.0, 1.1.0, Zenodo, doi:10.5281/zenodo.4624996
Brownlee, D. E., Horz, F., Newburn, R. L., et al. 2004, Sci, 304, 1764
Buzzi, L., Demetz, L., Aletti, A., et al. 2021, CBAT, 4989
Cochran, A. L., Levasseur-Regourd, A.-C., Cordiner, M., et al. 2015, SSRv, 197, 9
Cowan, J. J., & A'Hearn, M. F. 1979, M&P, 21, 155
Craig, M., Crawford, S., Seifert, M., et al. 2021, astropy/ccdproc: 2.2.0, 2.2.0, Zenodo, doi:10.5281/zenodo.4883632
Farnham, T. L., Kelley, M. S. P., & Bauer, J. M. 2021, PSJ, 2, 236
Ginsburg, A., Sipőcz, B. M., Brasseur, C. E., et al. 2019, AJ, 157, 98
Giorgini, J. D., Yeomans, D. K., Chamberlin, A. B., et al. 1996, BAAS, 28, 1158
Hui, M.-T., Farnocchia, D., & Micheli, M. 2019, AJ, 157, 162
Hui, M.-T., Jewitt, D., & Clark, D. 2018, AJ, 155, 25
Hui, M.-T., Jewitt, D., Yu, L.-L., & Mutchler, M. J. 2022, ApJL, 929, L12
Ishiguro, M., Kuroda, D., Hanayama, H., et al. 2016, AJ, 152, 169
Ivezić, Ž., Smith, J. A., Miknaitis, G., et al. 2007, AJ, 134, 973
Jewitt, D. 2015, AJ, 150, 201
Jewitt, D., Hui, M.-T., Mutchler, M., et al. 2017, ApJL, 847, L19
Joye, W. A., & Mandel, E. 2003, in ASP Conference Series, Vol. 295, Astronomical Data Analysis Software and Systems XII, ed. H. E. Payne, R. I. Jedrzejewski, & R. N. Hook (San Francisco, CA: ASP), 489
Kaib, N. A. 2022, SciA, 8, eabm9130
Kelley, M. S. P., & Lister, T. 2019, Calviacat: Calibrate star photometry by comparison to a catalog, 1.0.2, Zenodo, doi:10.5281/zenodo.2635841
Kelley, M. S. P., Lister, T., & Holt, C. E. 2021, ATel, 14917, 1
Kokotanekova, R., Lister, T., Bannister, M., et al. 2021a, ATel, 14733, 1
Kokotanekova, R., Opitom, C., Knight, M., et al. 2021b, BAAS, 53, 301
Kramer, E. A., Fernandez, Y. R., Lisse, C. M., Kelley, M. S. P., & Woodney, L. M. 2014, Icar, 236, 136

Lellouch, E., Moreno, R., Bockelée-Morvan, D., Biver, N., & Santos-Sanz, P. 2022, A&A, 659, L1

Lister, T., Kelley, M. S. P., Holt, C. E., et al. 2022, PSJ, in press

Lister, T. A., Gomez, E., Chatelain, J., et al. 2021, Icar, 364, 114387

McCully, C., Volgenau, N. H., Harbeck, D. R., et al. 2018, Proc. SPIE, 10707, 107070K

McCully, C., Turner, M., Volgenau, N., et al. 2018, LCOGT/banzai, 0.9.4, Zenodo, doi:10.5281/zenodo.1257560

Meech, K. J., & Svoreň, J. 2004, in Comets II, ed. M. C. Festou, H. U. Keller, & H. A. Weaver (Tucson, AZ: Univ. Arizona Press), 317

Meech, K. J., Kleyna, J. T., Hainaut, O., et al. 2017, ApJL, 849, L8

Mommert, M., Kelley, M., de Val-Borro, M., et al. 2019, JOSS, 4, 1426

Ridden-Harper, R., Bannister, M. T., & Kokotanekova, R. 2021, RNAAS, 5, 161

Robitaille, T., Deil, C., & Ginsburg, A. 2020, asclsoft: 2011.023

Ruprecht, J. D., Bosh, A. S., Person, M. J., et al. 2015, Icar, 252, 271

Schleicher, D. G., & Bair, A. N. 2011, AJ, 141, 177

Solontoi, M., Ivezić, Ž., Jurić, M., et al. 2012, Icar, 218, 571

Tonry, J. L., Stubbs, C. W., Lykke, K. R., et al. 2012, ApJ, 750, 99

Tonry, J. L., Denneau, L., Flewelling, H., et al. 2018, ApJ, 867, 105

Tubiana, C., Snodgrass, C., Bertini, I., et al. 2015, A&A, 573, A62

Van Selous, M., & Kelley, M. S. P. 2021, Small-Bodies-Node/Ice-Sublimation, GitHub, Commit, https://github.com/Small-Bodies-Node/ice-sublimation

Veverka, J., Klaasen, K., A'Hearn, M., et al. 2013, Icar, 222, 424

Vincent, J.-B., Bodewits, D., Besse, S., et al. 2015, Natur, 523, 63

Vokrouhlický, D., Nesvorný, D., & Dones, L. 2019, AJ, 157, 181

Wierzchos, K., & Womack, M. 2020, AJ, 159, 136

Wierzchos, K., Womack, M., & Sarid, G. 2017, AJ, 153, 230

Willmer, C. N. A. 2018, ApJS, 236, 47

Womack, M., Sarid, G., & Wierzchos, K. 2017, PASP, 129, 031001

Yang, B., Jewitt, D., Zhao, Y., et al. 2021, ApJL, 914, L17